

Planning and Learning Using Adaptive Entropy Tree Search

Piotr Kozakowski,¹ Mikołaj Pacek,¹ Piotr Miłoś²

¹ Faculty of Mathematics, Informatics and Mechanics, University of Warsaw

² Institute of Mathematics of the Polish Academy of Sciences

p.kozakowski@mimuw.edu.pl, m.pacek2@student.uw.edu.pl, pmilos@impan.pl

Abstract

We present the Adaptive Entropy Tree Search (ANTS) algorithm, a planning method based on the Principle of Maximum Entropy. Importantly, we design ANTS so that it is a practical component of a planning-learning loop, outperforming state-of-the-art methods on the Atari benchmark. The key algorithmic novelty is entropy parameterization, which mitigates sensitivity to the temperature parameter - a bottleneck of the prior maximum entropy planning methods. To confirm our design choices, we perform a comprehensive suite of ablations in isolation from learning. Moreover, we theoretically show that ANTS enjoys exponential convergence in the softmax bandit setting.

Introduction

Planning is one of the main approaches to sequential decision-making (Russell and Norvig 2009). A particularly successful planning method is Monte Carlo Tree Search (MCTS) (Kocsis and Szepesvári 2006; Browne et al. 2012) - an algorithm using value estimates to iteratively expand the search tree in the most promising directions. MCTS is very versatile, finding applications ranging from playing complex strategic games (Lee et al. 2009), through testing security systems (Tanabe, Yoshizoe, and Imai 2009), physics simulations (Mansley, Weinstein, and Littman 2011), production management (Chaslot et al. 2006), to creative content generation (Mahlmann, Togelius, and Yannakakis 2011).

An auspicious direction of research is the combination of MCTS with deep learning. It has already powered one of the breakthroughs in the recent history of AI: AlphaZero (Silver et al. 2018), a system combining planning and learning to master Go - a game known for its strategic complexity. Search and learning can be thought of as two complementary approaches to generate intelligent behavior (Bengio, Lodi, and Prouvost 2021). On the one hand, search can discover high-quality decisions, but falls short in large state spaces. On the other hand, learning can harness powerful pattern matching techniques and discover useful state representations, but cannot use additional online computation. Utilizing learning can significantly reduce the search space and guide planning to make it significantly more efficient (Silver et al. 2018; Agostinelli et al. 2019).

The Principle of Maximum Entropy (PME) is closely related to the probability matching strategy (Vulkan 2000)

and has been shown to accurately model collective human behavior (Ziebart 2018; Hernando et al. 2013). In the reinforcement learning context, PME provides robustness against reward uncertainty and adversity (Eysenbach and Levine 2019). As such, it can possibly be used to implement uncertainty as to the true objective; a property argued to be instrumental in designing AI systems that align with human goals (Hadfield-Menell et al. 2017). Importantly, PME has powered successful and practical algorithms (Haarnoja et al. 2017, 2018) and recently inspired planning methods (Xiao et al. 2019; Dam et al. 2020).

Due to its modular structure, MCTS lends itself for various modifications (Browne et al. 2012). In particular, PME can be incorporated, as done in Xiao et al. (2019); Dam et al. (2020). Such a blend results in successful planning algorithms with good theoretical guarantees. An important obstacle inhibiting their practical adoption is high sensitivity to the temperature hyperparameter, whose optimal value can vary significantly from task to task, and even within a single episode (Haarnoja et al. 2019). Our approach, Adaptive Entropy Tree Search (ANTS), combines several techniques that considerably improve the performance of maximum entropy Monte Carlo planning, including dynamic adaptation of the temperature. ANTS adjusts the temperature to reach a desired level of entropy within the planning tree. In addition to being less sensitive, this parameterization has a more intuitive interpretation: the Shannon entropy of a discrete distribution can be regarded as a logarithm of its *weighted average branching factor* (Jurafsky and Martin 2020). As such, by setting the level of entropy, we control the breadth of the search tree.

Algorithms in Xiao et al. (2019); Dam et al. (2020) utilize pretrained Q-value networks, which necessitates expert data. We remove this restrictive assumption and deliver a full planning-learning loop akin to AlphaZero (Silver et al. 2018). Our contributions are two-fold. First, we make an extensive empirical evaluation of the previous methods. We determine the high sensitivity to the temperature hyperparameter to be a critical bottleneck. Secondly, we propose a temperature adaptation mechanism and several other advancements, which together yield a planning-learning method capable of delivering state-of-the-art results. In more detail:

1. We present a novel algorithm, Adaptive Entropy Tree Search. We show that ANTS is a very effective compo-

ment of a planning-learning loop akin to AlphaZero (Silver et al. 2018). It significantly outperforms the maximum entropy planning baselines MENTS and TENTS, as well as the state-of-the-art PUCT algorithm on the Atari benchmark. To the best of our knowledge, this is *the first evaluation of maximum entropy MCTS methods in planning-learning loops*.

2. We present an extensive empirical study, evaluating the planning capabilities of our approach in isolation from learning, in comparison with MENTS, TENTS and PUCT. A key finding is that the parameterization via entropy, employed by ANTS, exhibits superior robustness to hyperparameter choices.
3. We prove that under mild assumptions, dynamic temperature adaptation retains the exponential convergence rate of the E2W sampling strategy, used in MENTS, in the context of softmax bandits.

Background

Reinforcement learning and planning

Reinforcement learning (RL) focuses on solving sequential decision problems formalized as Markov decision processes (MDPs). We consider a discounted, finite-horizon MDP, which is defined as a 5-tuple $\langle \mathcal{S}, \mathcal{A}, \mathcal{P}, \mathcal{R}, \gamma \rangle$, where \mathcal{S} is the set of states, \mathcal{A} is the set of actions, $\mathcal{P}(s'|s, a)$ is the transition distribution, $\mathcal{R} : \mathcal{S} \times \mathcal{A} \rightarrow \mathbb{R}$ is the reward function and $\gamma \in [0, 1)$ is the discount factor. We assume deterministic rewards for simplicity, but all our considerations apply to stochastic rewards as well. We define a *policy* $\pi(a|s)$ as a state-dependent distribution over actions. For a given policy π , we define the *state value function* as $V^\pi(s) = \mathbb{E}_{(s_t, a_t)_{t=0}^\infty} [\sum_{t=0}^\infty \gamma^t \mathcal{R}(s_t, a_t)]$, where $s_0 = s$, $a_t \sim \pi(\cdot|s_t)$, $s_{t+1} \sim \mathcal{P}(\cdot|s_t, a_t)$ - the expected cumulative return obtained by π when starting from state s . We define the *state-action value function* as $Q(s, a) = \mathcal{R}(s, a) + \gamma \mathbb{E}_{s' \sim \mathcal{P}(\cdot|s, a)} V(s')$ - the expected cumulative return obtained by executing action a in state s and then continuing using π .

RL methods aim to find an optimal policy π^* by *learning* from trajectories sampled from the MDP. The optimal state value function $V^* = V^{\pi^*}$ and state-action value function, also called *Q-function*, $Q^* = Q^{\pi^*}$ satisfy a recursive relationship known as the Bellman optimality equations (Sutton and Barto 2018, Section 3.6): $V^*(s) = \max_{a \in \mathcal{A}} Q^*(s, a)$, $Q^*(s, a) = \mathcal{R}(s, a) + \gamma \mathbb{E}_{s' \sim \mathcal{P}(\cdot|s, a)} V^*(s')$. An optimal policy is a *greedy policy* with respect to the optimal state-action value function: $\pi^*(a|s) = \operatorname{argmax}_{a \in \mathcal{A}} Q^*(s, a)$. Model-based RL additionally assumes access to a *model* of the MDP $\mathcal{P}'(s'|s, a)$, which is typically used to consider multiple rollouts from a given state, in a process known as *planning*. In this work, we assume access to the perfect model of the MDP, that is $\mathcal{P}' = \mathcal{P}$.

Monte Carlo Tree Search

Monte Carlo Tree Search (MCTS) is a class of planning algorithms for discrete action spaces (Browne et al. 2012). MCTS iteratively builds a planning tree in which nodes correspond to states and edges correspond to (state, action)

pairs. MCTS estimates values of the nodes by aggregating multiple paths ending at leaves. The algorithm consists of four phases, repeated in a loop:

1. **Selection**, in which a path from the root to a leaf is selected.
2. **Expansion**, in which a successor state of the selected leaf is added to the tree as a new leaf.
3. **Simulation**, in which the value of the new leaf is estimated using random rollouts.
4. **Backpropagation**, in which the value estimates of nodes on the path are updated, starting from the bottom.

Numerous improvements to MCTS have been developed over the years. Notably, Silver et al. (2018) supplement MCTS with neural networks. In the selection phase, the next node is selected to maximize

$$\text{PUCT}(s, a) = Q(s, a) + c \pi_{\text{prior}}(a|s) \frac{\sqrt{N(s)}}{N(s, a) + 1} \quad (1)$$

from the current node s , where $c > 0$ is an exploration parameter, $\pi_{\text{prior}}(a|s)$ is a prior policy, $N(s)$ is the number of visits in state s and $N(s, a)$ is the number of times action a has been executed in state s . In the simulation phase, the value of a leaf s is estimated using a neural network. The prior policy is also provided by a neural network, trained to predict the distribution of actions selected during planning: $\frac{N(s, a)}{N(s)}$. The value network is trained to estimate the empirical state values $V(s)$.

In this work, we consider an expansion phase that adds all successors of a given node to the tree at the same time. Those new leaves are initialized using a *Q-network* $\hat{Q}(s, a)$. This is an optimization suitable for problems in which computing state transitions is expensive, such as tasks from the Atari benchmark utilized in this work. The *Q-network* is trained to estimate the empirical state-action values $Q(s, a)$.

When evaluating the algorithm using a pretrained network, the action to take after planning can be chosen according to the maximum visitation count: $a(s) = \operatorname{argmax}_{a \in \mathcal{A}} N(s, a)$, a procedure employed by Silver et al. (2018). When collecting episodes for training the network, we must ensure proper exploration, so the training data is diverse enough. In this case, we can introduce an additional parameter: action selection temperature $\tau_{\text{sel}} \in (0, 1)$, and sample from the action visitation distribution sharpened by this temperature:

$$\pi(a|s) \propto \exp\left(\frac{1}{\tau_{\text{sel}}} \log N(s, a)\right). \quad (2)$$

This approach was taken by Schrittwieser et al. (2020) in their Atari experiments.

Maximum entropy RL

Maximum entropy RL is the application of the Principle of Maximum Entropy to reinforcement learning. It has recently given rise to a number of successful algorithms (Haarnoja et al. 2017, 2018; Hausman et al. 2018). It augments the RL objective with an entropy regularization term, rewarding

uncertainty of the policy and thus promoting exploratory behaviors:

$$J(\pi) = \mathbb{E}_{(s_t, a_t)_{t=0}^{\infty}} \left[\sum_{t=0}^{\infty} \gamma^t [\mathcal{R}(s_t, a_t) + \tau \mathcal{H}(\pi(\cdot|s_t))] \right] \quad (3)$$

where \mathcal{H} is Shannon entropy and $\tau > 0$ is a temperature parameter, regulating the amount of exploration. We denote the solution to the entropy-regularized RL objective as $\pi^* = \operatorname{argmax}_{\pi} J(\pi)$.

Haarnoja et al. (2017) derive a backup operator, which can be used to solve entropy-regularized RL problems:

$$\begin{aligned} Q(s, a) &\leftarrow \mathcal{R}(s, a) + \gamma \mathbb{E}_{s' \sim \mathcal{P}(\cdot|s, a)} V(s') \\ V(s) &\leftarrow \tau \log \sum_{a \in \mathcal{A}} \exp \left(\frac{1}{\tau} Q(s, a) \right), \end{aligned} \quad (4)$$

Fixed point iteration on this backup results in $Q = Q^*$, $V = V^*$, from which the optimal policy can be recovered: $\pi^*(\cdot|s) = \exp \left(\frac{1}{\tau} (Q^*(s, a) - V^*(s)) \right)$.

Xiao et al. (2019) utilize (4) within the MCTS framework. In the selection phase, the consecutive nodes are chosen using the E2W sampling strategy proposed by the authors. In the simulation phase, leaves are initialized using a Q -network. In the backpropagation phase, node state values and Q -values are updated according to (4).

Dam et al. (2020) generalize E2W to other types entropy, resulting in the E3W sampling strategy. They derive two new planning methods based on this procedure: TENTS, based on Tsallis entropy, and RENTS, based on relative entropy. Both E2W and E3W use the same formula:

$$\begin{aligned} \pi_{\tau}^{\text{e3w}}(a|s) &= (1 - \lambda_s) \pi_{\tau}(a|s) + \lambda_s \frac{1}{|\mathcal{A}|}, \\ \pi_{\tau}(a|s) &\propto \exp \left(\frac{1}{\tau} Q(s, a) \right), \\ \lambda_s &= \frac{\epsilon |\mathcal{A}|}{\log(N(s) + 1)}, \epsilon > 0. \end{aligned} \quad (5)$$

The generalization of E2W into E3W utilizes the Legendre-Fenchel transform, described in the Appendix. For simplicity, in the formulas in this work we assume Shannon entropy, but our method works with Tsallis entropy as well, as demonstrated in the **Experiments**.

Method

We now describe our method, Adaptive Entropy Tree Search (ANTS). We follow the general template of MENTS and TENTS, augmented by temperature adaptation and several other improvements described below. In addition to the evaluation using pretrained Q -networks, investigated in (Xiao et al. 2019; Dam et al. 2020), we extend ANTS to work in the more practical setting of a planning-learning loop. In subsection **Planning and learning** we describe techniques which enable this extension. The pseudocode of the algorithm is presented in the Appendix.

Temperature adaptation

In our method, the temperature τ is chosen considering entropies (depending on τ) of nodes expanded by the MCTS planner (denoted by $\mathcal{S}_{\text{tree}}$). Different values of the temperature are assigned not only for different tasks and different episodes of the same task, but varied within a single episode. This feature may be helpful in tasks consisting of semantically distinct parts that would require different exploration strategies.

Specifically, τ is varied so that the mean node entropy matches the prescribed value \mathcal{H}_{avg} . This is achieved by finding a root of the following function:

$$\mathcal{H}^+(\tau) = \left[\frac{1}{|\mathcal{S}_{\text{tree}}|} \sum_{s \in \mathcal{S}_{\text{tree}}} \mathcal{H}(\pi_{\tau}(\cdot|s)) \right] - \mathcal{H}_{\text{avg}}, \quad (6)$$

$$\text{where } \pi_{\tau}(a|s) \propto \exp \left(\frac{1}{\tau} Q(s, a) \right). \quad (7)$$

For $\mathcal{H}_{\text{avg}} \in (0, \mathcal{H}_{\text{max}})$, where \mathcal{H}_{max} denotes the maximum possible entropy of a policy in the given action space, $\mathcal{H}^+(\tau)$ always has a root. Indeed, as $\tau \searrow 0$, the policies become deterministic, so the mean entropy approaches 0. When $\tau \nearrow \infty$, they become uniform, so the mean entropy approaches \mathcal{H}_{max} . To avoid numerical issues when $\tau \approx 0$, we impose a lower bound on the temperature: τ_{min} . Any root-finding algorithm can be applied here. For simplicity, we use the derivative-free Brent algorithm (Brent 1973).

In order to avoid instabilities, we smooth the temperature using exponential moving average. We smooth in log-space to be able to quickly adapt the order of the magnitude:

$$\log \tilde{\tau}_{i+1} = \alpha \log \tilde{\tau}_i + (1 - \alpha) \log \tau_{i+1}, \quad \alpha > 0, \quad (8)$$

where i is the number of the adaptation phase, and τ_i is obtained from temperature adaptation. At the beginning, we set the temperature to a high value τ_0 to ensure broad exploration in the initial stage of planning. We adapt the temperature every fixed number of planning passes. After each adaptation phase, we recalculate the values of nodes using the new temperature $\tilde{\tau}_{i+1}$.

Simulation

In the simulation phase, we evaluate the newly-expanded leaves in the tree using a given Q -network. We initialize their Q -values as

$$Q(s, a) \leftarrow \hat{Q}(s, a), \quad (9)$$

where \hat{Q} denotes the Q -network. This stands in contrast to the MENTS and TENTS algorithms, in which the leaves are initialized by

$$\begin{aligned} Q(s, a) &\leftarrow \left(\hat{Q}(s, a) - \hat{V}(s) \right) / \tau_{\text{init}}, \\ \hat{V}(s) &= \tau \log \sum_{a \in \mathcal{A}} \exp \left(\frac{1}{\tau} Q(s, a) \right), \end{aligned} \quad (10)$$

where τ_{init} is a hyperparameter separate from the entropy regularization temperature τ . We discovered that our simpler initialization method yields considerable improvement, as demonstrated in section Ablations.

Backpropagation

In the backpropagation phase, we use a modification of (4):

$$V(s) \leftarrow \tau \log \sum_{a \in \mathcal{A}} \exp\left(\frac{1}{\tau} Q(s, a)\right) - \tau \mathcal{H}_{\max}, \quad (11)$$

where \mathcal{H}_{\max} is the maximum possible entropy. This modification is designed to prevent the inefficient depth-first behavior, which we observed in our initial experiments. Since values calculated by (4) include positive entropy pseudorewards, they overestimate the true returns. We observed that as a result, the planner can start deepening the same, single path, because it keeps receiving high values along it. The pseudoreward shaping term $-\tau \mathcal{H}_{\max}$ mitigates this phenomenon. We note that as the subtracted value does not depend on the action, this shaping does not change the optimal policy obtained at infinite computational budget.

Planning and learning

The ultimate goal of this paper is to put the ANTS algorithm in a planning-learning loop. The loop is similar to the (Silver et al. 2018); we describe it in detail below. We stress that our algorithmic developments, presented above, and learning details below were critical to making the planning-learning setting efficient.

The loop consists of two phases: data collection and training. In the first phase the planner is run for several episodes, using a neural network for initializing the Q -values of leaves added to the tree. The episodes, along with state Q -values calculated by the planner, are stored in a replay buffer and used to train the neural network in the next phase. We note that the planner Q -values are typically more accurate than the ones by from the network; this difference provides learning signal.

During data collection, we use an exploration scheme similar to (2). Actions performed at each step in the environment are sampled from:

$$\pi(a|s) = \pi_{\tau \cdot \tau_{\text{sel}}}^{\text{E3W}}(a|s), \quad (12)$$

where $\tau_{\text{sel}} \in (0, 1)$ is an action selection temperature parameter. We use it to interpolate between the E3W (5) and the argmax policy: $a(s) = \operatorname{argmax}_{a \in \mathcal{A}} Q(s, a)$.

Another important element is accommodating for temperature changes during training. For this purpose, we inject information about the current temperature to the network - the learning targets are influenced by this value. We have discovered that giving the network access to this information greatly stabilizes the algorithm. More details are provided in the Appendix.

Theoretical analysis

The exponential convergence result for E2W in the softmax bandit problem, formulated and proven by Xiao et al. (2019), still holds when the temperature changes, under the following conditions:

1. The temperature τ_t in adaptation step t converges to τ at rate $|\tau_t - \tau| = O(1/\log t)$. We note that since it is a very slow convergence rate, this assumption is easily satisfied in practice.

2. The reward distribution is sub-Gaussian. The same assumption is required for exponential convergence of E2W with constant temperature (Xiao et al. 2019).

The formal statement of this result and its proof are described in the Appendix.

Related Work

Reinforcement Learning Recent years have brought significant advancements in reinforcement learning due to the use of powerful deep neural network (DNN) function approximators. Mnih et al. (2015) introduce DQN: Q-learning with DNNs, leading to human-level performance on the Arcade Learning Environment (Bellemare et al. 2012). The algorithmic progress has been perhaps equally important. Hessel et al. (2018) combine multiple improvements to DQN, enabling superior performance across the ALE benchmark. Badia et al. (2020) advance even further, leading to an algorithm that achieves superhuman performance on all 57 ALE tasks. Model-based RL methods assume access to a model of the MDP. The classical work of Sutton (1991) introduces a method of learning the model alongside the agent, which is then used to generate imaginary experience for RL training. Łukasz Kaiser et al. (2020) apply a similar approach to the ALE benchmark, establishing state-of-the-art in performance in the low budget of 100K interactions with the environment. Ha and Schmidhuber (2018) present a method of planning in the latent space of a learned model. Hafner et al. (2020) plan by propagating gradients through the latent states of a learned model.

Monte Carlo Tree Search MCTS is a combination of the UCB strategy for multi-armed bandits with tree search (Kocsis and Szepesvári 2006). Browne et al. (2012) provide a survey of methods in the MCTS family. Silver et al. (2018) introduce AlphaZero - MCTS powered with neural networks and self-play, to obtain a system achieving superhuman performance in complex strategic board games: chess, shogi and go. Schrittwieser et al. (2020) develop MuZero, an extension of AlphaZero with a learned model, and establish new state-of-the-art on ALE. Hamrick et al. (2021) provide an extensive empirical analysis of MuZero, shedding light on the role of planning in model-based RL.

Each phase of the MCTS algorithm (selection, expansion, simulation, backpropagation) can be replaced and improved, which gives rise to a plethora of related methods. Grill et al. (2020) find a connection between MCTS and policy optimization, which they use to derive a novel selection rule. Kozakowski et al. (2020) regulate the bias-variance trade-off by expanding multiple consecutive leaves along a path. Hamrick et al. (2020) perform simulation (leaf initialization) using neural networks trained via Q-learning. Miłoś et al. (2020) use ensembles of neural networks for uncertainty-aware simulation. Khandelwal et al. (2016) use the intuitions from TD- λ value estimation (Sutton 1988) to derive new backpropagation rules for MCTS.

Maximum Entropy RL The Principle of Maximum Entropy (PME) has shown success in modeling human behavior (Ziebart 2018). Levine (2018) describe the maximum entropy RL problem as inference in a probabilistic graphical

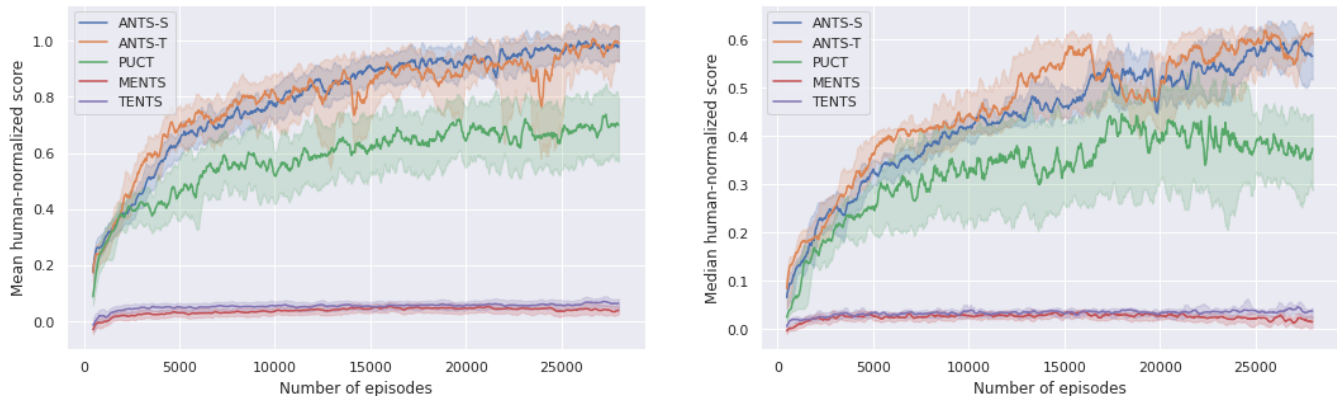


Figure 1: Learning curves of the planning-learning loop experiments. Each plot represents the mean or median over the 21 games of the human-normalized score. Bold lines denote a median of five seeds. Shaded regions denote the interquartile range. Each point corresponds to a mean of 24 episodes. Each episode is run for a maximum of 1000 interactions. The curves are smoothed by rolling mean of 10 points.

model. Ziebart et al. (2008) apply the PME to inverse reinforcement learning, and pose the problem of imitation learning as finding an optimal maximum entropy policy in the constructed MDP. Eysenbach and Levine (2019) analyze the maximum entropy RL problem and show its equivalence to classes of MDPs with uncertain or adversarial reward functions. (Nachum et al. 2017) establish a connection between policy-based and value-based RL under entropy regularization. Haarnoja et al. (2017) introduce Soft Q-Learning: a deep RL method derived from soft Q-iteration (4). Haarnoja et al. (2018) present another maximum entropy RL method: Soft Actor-Critic (SAC), achieving state-of-the-art performance in continuous control tasks. Hausman et al. (2018) establish a variational lower bound for the entropy pseudo-reward to learn an embedding space of transferable robotic skills. Haarnoja et al. (2019) derive a method of automatically adapting the temperature parameter of SAC. Xiao et al. (2019) use the maximum entropy framework to derive E2W: an optimal sampling strategy for the softmax stochastic bandit problem, and introduce MENTS - an MCTS algorithm using this strategy in the selection phase. Dam et al. (2020) extend E2W to different types of entropy: Tsallis entropy and relative Shannon entropy.

Experiments

We present the results of ANTS combined with two types of entropy: ANTS-S using Shannon entropy, and ANTS-T using Tsallis entropy. As baselines, we include PUCT, MENTS and TENTS. PUCT denotes MCTS with the PUCT exploration bonus, utilized in the state-of-the-art planning system AlphaZero (Silver et al. 2018). We run our experiments on a set of 21 Atari games and using the perfect model of the environment, in a setting similar to Dam et al. (2020).

In our main series of experiments, we train the Q -networks in a closed loop of planning and learning. For training we utilize Q -value targets calculated by the planner, in a similar fashion to Silver et al. (2018). We then present experiments with Q -networks pretrained using DQN for leaf

initialization, as done in Xiao et al. (2019) and Dam et al. (2020). Next, we provide an empirical comparison between two parameterizations of maximum entropy planning: via temperature and via entropy. Finally, we present ablations of various components of ANTS using pretrained Q -networks. Additionally, we provide visualizations of temperature adaptation in the Appendix.

To ensure fair comparison, we run extensive hyperparameter tuning of all presented methods, using equal computational budget, see details in the Appendix. The code and hyperparameter settings used to run all experiments in this work are included in the supplementary material.

Planning-learning loop

In this section we present experiments showing that ANTS augmented with learning significantly exceeds the results of MENTS and TENTS in this setting. Moreover, it outperforms the state-of-the-art PUCT (utilized in AlphaZero), at the same time being more stable, as shown in Figure 1. To the best of our knowledge, this is the first such demonstration for maximum entropy MCTS methods.

In these experiments we use a relatively modest computational budget per episode, setting the number of MCTS simulations to 30 and limit the depth of the search tree to 20. An important technical step towards stabilizing training was providing the current temperature as an additional input to the Q -network, as described in section **Method**. In order to collect diverse data for network training, we employ the exploration strategy (12) for ANTS, MENTS and TENTS, and (2) for PUCT. The hyperparameter τ_{sel} is tuned for each method separately, as described in the Appendix. For each algorithm and game, we run five experiments, each collecting 28000 episodes in total. More details about the experimental setting are provided in the Appendix.

As we can see in Figure 1, the performances of both ANTS-S and ANTS-T consistently improve as they collect more data. Both algorithms exhibit similar performance, though ANTS-T appears slightly more sample efficient,

while ANTS-S is learns more steadily and has lower variance between seeds. PUCT learns slowly and unsteadily, and its median performance eventually starts to deteriorate. MENTS and TENTS completely fail, which confirms the importance of the improvements made in ANTS in the planning-learning loop setting.

Pretrained Q-networks

Table 1: **Results on Atari using pretrained Q-networks.** We report the mean of 100 episodes. Each episode is run for 10^4 interactions. For each environment, we bold the methods for which the difference with the highest score is not statistically significant (determined using a t -test with $p < 0.05$). The confidence intervals are provided in the Appendix.

	PUCT	MENTS	TENTS	ANTS-S	ANTS-T
Alien	2853	2590	2606	2783	2554
Amidar	137	251	236	148	184
Asterix	48506	8305	10406	51741	49758
Asteroids	3657	3786	3541	4059	3554
Atlantis	278156	275681	267429	277870	280492
BankHeist	680	543	472	707	715
BeamRider	21745	9424	7534	21268	18536
Breakout	389	306	243	351	377
Centipede	18662	59167	99631	51387	133842
DemonAttack	55947	49952	45960	53998	53462
Enduro	794	800	800	794	800
Frostbite	204	197	197	179	184
Gopher	9606	9330	8150	10770	10766
Hero	20715	19940	19845	20618	20443
MsPacman	3880	3873	3358	4923	4846
Phoenix	8875	6788	6857	9187	9557
Qbert	15120	13877	13815	15472	15223
Robotank	55	27	26	49	51
Seaquest	3270	1764	1533	2557	2656
SpaceInvaders	4630	2043	2024	4714	4453
WizardOfWor	11834	7063	8030	12937	13386

In Table 1 we present the results of experiments using pretrained Q-networks. This setup allows us to test the properties of the planners in isolation from learning. ANTS-S performs strongly, achieving the best result or a tie on 14 out of 21 games, on others being close to the best result. Our highly tuned PUCT presents a challenging baseline, outperforming both MENTS and TENTS in almost every case. Both ANTS-S and ANTS-T perform significantly better than MENTS and TENTS, which provides evidence that the improvements made in ANTS are beneficial also when the Q-network is supplied externally. Interestingly, the performance of both variants of ANTS using pretrained networks is on-par with PUCT, whereas in the planning-learning loop experiments ANTS performed better. These results give rise to a hypothesis that the advantage of ANTS over PUCT in planning-learning loops is caused by providing better data for training neural networks, rather than better planning using a given neural network.

In these experiments we use the same hyperparameters as in the previous section, with several adjustments. We use a

higher computational budget per episode: 100 MCTS simulations and search depth of 50. In ANTS, MENTS and TENTS we select an action with the maximum Q -value returned by the planner. In PUCT we select an action with the highest visitation count. Similarly to Xiao et al. (2019); Dam et al. (2020), we use networks pretrained with DQN for leaf initialization. For this purpose, we utilize the publicly available checkpoints from the Dopamine package (Castro et al. 2018).

Robustness

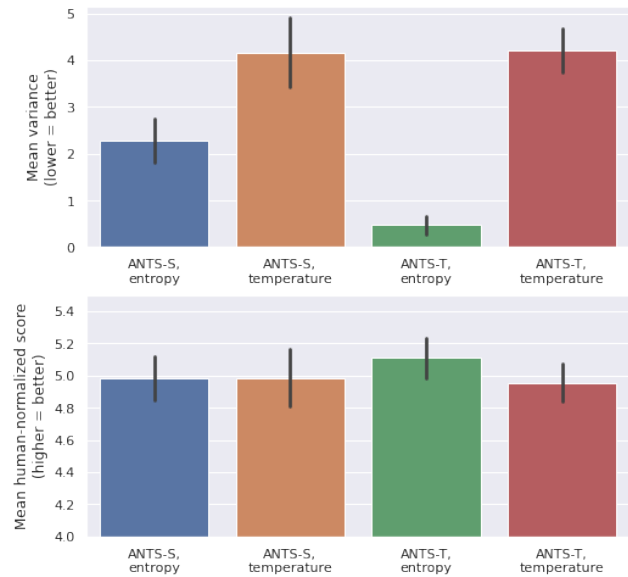


Figure 2: Robustness experiments on the 21 Atari games. We average over 24 episodes for each variant and game. Error bars denote 95% confidence intervals. ANTS-*, *entropy* denote the full ANTS algorithm. ANTS-*, *temperature* denote ANTS without temperature adaptation, keeping the temperature constant. These variants are equivalent to MENTS and TENTS with our simulation and backpropagation improvements described in section **Method**.

We now present a comparison of two parameterizations of maximum entropy planners: by mean entropy, used by ANTS, and by temperature, used by MENTS and TENTS. We evaluate the robustness to different parameter settings of the two parameterizations, as well as their performance when the hyperparameters are tuned. The results are shown in Figure 2, indicating the advantage of the entropy parameterization used by ANTS in both aspects. We additionally measure the performance without tuning, averaged over different hyperparameter values - see the Appendix.

Intuitively, an algorithm can be said to be robust to different hyperparameter choices, if its performance does not vary too much with different hyperparameter settings. To capture this intuition, we define our robustness metric as the variance of human-normalized scores attained at different hyperparameter values, where hyperparameters are chosen from a predefined set. We compute this metric separately for each

game, then average it over games:

$$\rho(A, H) = \mathbb{E}_{g \sim G} \text{Var}_{h \sim H} sc(A, h, g), \quad (13)$$

where A indicates the algorithm using a given parameterization, H is a set of its possible hyperparameter values, G is the set of games, \sim denotes sampling from the uniform distribution over a finite set, and $sc(A, h, g)$ is the score of algorithm A using hyperparameter h on game g .

To ensure fair comparison, the hyperparameter sets H should be of equal size and span the range of sensible values. For the temperature parameterization, the range of possible temperature values is $(0, \infty)$. To handle this infinite interval we choose temperatures equidistant in log-space, with endpoints selected to be the minimum and maximum temperature that worked best on some game. In the case of entropy parameterization, the interval is $(0, \mathcal{H}_{\max})$, where \mathcal{H}_{\max} depends on the entropy type and number of actions. We take values spanning this interval, equidistant in linear space.

As we can see in Figure 2, ANTS parameterized by entropy is more robust than the variant parameterized by temperature. In case of ANTS-S, mean variance of the entropy parameterization is 2 times lower than of the temperature parameterization. In case of ANTS-T, the difference is much greater: over 8 times. In terms of the absolute performance, ANTS-T parameterized by entropy is noticeably better than its temperature-parameterized counterpart. In case of ANTS-S, the difference is negligible.

Ablations

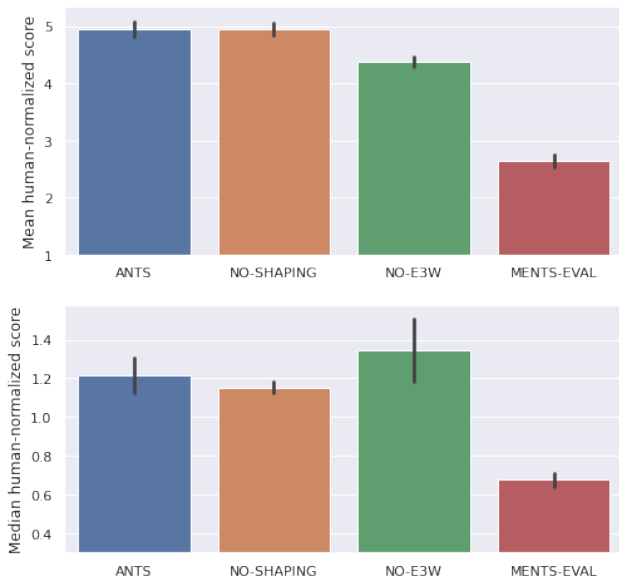


Figure 3: Ablations of ANTS-S on the 21 Atari games. We average over 24 episodes for each variant and game. Error bars denote 95% confidence intervals.

In order to measure the contribution of the different components of ANTS, we perform additional experiments with pretrained networks, removing the individual features of our method. For each variant we report the mean and median

human-normalized score. The results are shown in Figure 3. ANTS denotes the full algorithm using Shannon entropy. NO-SHAPING denotes ANTS without pseudoreward shaping and MENTS-EVAL denotes a variant of ANTS where leaf initialization is performed using (10), as done in Xiao et al. (2019) and Dam et al. (2020). We additionally include NO-E3W, denoting ANTS that samples directly from $\pi(a|s) \propto \exp(Q(s, a)/\tau)$ during the selection phase, instead of using E3W. The ablations use the same base hyperparameter set as in section **Pretrained Q-networks**. In the MENTS-EVAL experiment we re-tune τ_{init} jointly on all games, maximizing the mean human-normalized score. In both cases, we use the same set of hyperparameter values as when tuning MENTS. More details about hyperparameter tuning are included in the Appendix.

In Figure 3 we can see that leaf initialization using raw outputs of the Q-network plays the largest role out of the evaluated components of ANTS. One possible explanation is that leaf initialization using formula (10) retains only information about relations between actions, losing information about the absolute value of a state. This could prevent the planner from meaningful comparison of nodes higher in the tree. In the case of pseudoreward shaping, the difference is less apparent and only visible in the median human-normalized score plot. Interestingly, NO-E3W performs worse than ANTS in terms of mean score and better in terms of median score. It appears that E3W sampling is necessary on a small number of games, which escalates the mean score, but hurts on most games, which diminishes the median score. It is also worth noticing that the median NO-E3W score has considerably higher variance.

Conclusions

In this work, we have presented Adaptive Entropy Tree Search: a method combining several improvements to maximum entropy Monte Carlo planning, including temperature adaptation. In the planning-learning setting, ANTS delivers superior performance and stability compared to the state-of-the-art PUCT. Moreover, ANTS is on par with PUCT when used as a standalone planner, with pretrained neural networks. Importantly, ANTS considerably improves upon the related MENTS and TENTS algorithms in both aspects. We have demonstrated that the entropy reparameterization introduced by ANTS leads to increased robustness to hyperparameter settings. We have analyzed the components of ANTS in a comprehensive ablation study and provided theoretical motivation for temperature adaptation in maximum entropy planning. We believe that a promising direction for future research is further analysis of maximum entropy approaches in planning-learning loops. The high performance of ANTS in this setting can be attributed to good exploration or exploitation. Both can play a role - on the one hand, maximum entropy planning can be seen as an alternative method of exploration to UCT/PUCT; on the other hand, maximum entropy RL approaches are believed to aid in smoothing the optimization landscape of neural networks (Ahmed et al. 2019). We believe that this line of research would serve as a step towards developing practical planning approaches to challenging real-world problems.

Acknowledgments

The work of Piotr Kozakowski was supported by the Polish National Science Center grant 2020/37/N/ST6/04113. The work of Piotr Miłoś was supported by the Polish National Science Center grant 2017/26/E/ST6/00622. This research was supported by the PL-Grid Infrastructure. Our experiments were managed using <https://neptune.ai>. We would like to thank the Neptune team for providing us access to the team version and technical support.

References

- Abadi, M.; Barham, P.; Chen, J.; Chen, Z.; Davis, A.; Dean, J.; Devin, M.; Ghemawat, S.; Irving, G.; Isard, M.; Kudlur, M.; Levenberg, J.; Monga, R.; Moore, S.; Murray, D. G.; Steiner, B.; Tucker, P.; Vasudevan, V.; Warden, P.; Wicke, M.; Yu, Y.; and Zheng, X. 2016. TensorFlow: A System for Large-Scale Machine Learning. In *Proceedings of the 12th USENIX Conference on Operating Systems Design and Implementation, OSDI'16*, 265–283. USA: USENIX Association. ISBN 9781931971331.
- Agostinelli, F.; McAleer, S.; Shmakov, A.; and Baldi, P. 2019. Solving the Rubik’s cube with deep reinforcement learning and search. *Nature Machine Intelligence*, 1(8): 356–363.
- Ahmed, Z.; Le Roux, N.; Norouzi, M.; and Schuurmans, D. 2019. Understanding the Impact of Entropy on Policy Optimization. In Chaudhuri, K.; and Salakhutdinov, R., eds., *Proceedings of the 36th International Conference on Machine Learning*, volume 97 of *Proceedings of Machine Learning Research*, 151–160. PMLR.
- Ba, J. L.; Kiros, J. R.; and Hinton, G. E. 2016. Layer Normalization. arXiv:1607.06450.
- Badia, A. P.; Piot, B.; Kapturowski, S.; Sprechmann, P.; Vitvitskiy, A.; Guo, Z. D.; and Blundell, C. 2020. Agent57: Outperforming the Atari Human Benchmark. In III, H. D.; and Singh, A., eds., *Proceedings of the 37th International Conference on Machine Learning*, volume 119 of *Proceedings of Machine Learning Research*, 507–517. PMLR.
- Bellemare, M. G.; Naddaf, Y.; Veness, J.; and Bowling, M. 2012. The Arcade Learning Environment: An Evaluation Platform for General Agents. *Journal of Artificial Intelligence Research*, Vol. 47: 253–279. Cite arxiv:1207.4708.
- Bengio, Y.; Lodi, A.; and Prouvost, A. 2021. Machine learning for combinatorial optimization: A methodological tour d’horizon. *European Journal of Operational Research*, 290(2): 405–421.
- Brent, R. 1973. *Algorithms for minimization without derivatives*. Prentice-Hall. ISBN 0-13-022335-2.
- Brockman, G.; Cheung, V.; Pettersson, L.; Schneider, J.; Schulman, J.; Tang, J.; and Zaremba, W. 2016. OpenAI Gym. arXiv:1606.01540.
- Browne, C.; Powley, E.; Whitehouse, D.; Lucas, S.; Cowling, P.; Rohlfshagen, P.; Tavener, S.; Perez Liebana, D.; Samothrakis, S.; and Colton, S. 2012. A Survey of Monte Carlo Tree Search Methods. *IEEE Transactions on Computational Intelligence and AI in Games*, 4:1: 1–43.
- Castro, P. S.; Moitra, S.; Gelada, C.; Kumar, S.; and Bellemare, M. G. 2018. Dopamine: A Research Framework for Deep Reinforcement Learning. arXiv:1812.06110.
- Chaslot, G.; Jong, S.; Saito, J.-T.; and Uiterwijk, J. 2006. Monte-Carlo Tree Search in Production Management Problems. *Belgian/Netherlands Artificial Intelligence Conference*.
- Dam, T.; D’Eramo, C.; Peters, J.; and Pajarinen, J. 2020. Convex Regularization in Monte-Carlo Tree Search. arXiv:2007.00391.
- Eysenbach, B.; and Levine, S. 2019. If MaxEnt RL is the Answer, What is the Question? arXiv:1910.01913.
- Grill, J.-B.; Altché, F.; Tang, Y.; Hubert, T.; Valko, M.; Antonoglou, I.; and Munos, R. 2020. Monte-Carlo Tree Search as Regularized Policy Optimization. In III, H. D.; and Singh, A., eds., *Proceedings of the 37th International Conference on Machine Learning*, volume 119 of *Proceedings of Machine Learning Research*, 3769–3778. PMLR.
- Ha, D.; and Schmidhuber, J. 2018. Recurrent World Models Facilitate Policy Evolution. In Bengio, S.; Wallach, H.; Larochelle, H.; Grauman, K.; Cesa-Bianchi, N.; and Garnett, R., eds., *Advances in Neural Information Processing Systems*, volume 31, 2450–2462. Curran Associates, Inc.
- Haarnoja, T.; Tang, H.; Abbeel, P.; and Levine, S. 2017. Reinforcement Learning with Deep Energy-Based Policies. In Precup, D.; and Teh, Y. W., eds., *Proceedings of the 34th International Conference on Machine Learning*, volume 70 of *Proceedings of Machine Learning Research*, 1352–1361. International Convention Centre, Sydney, Australia: PMLR.
- Haarnoja, T.; Zhou, A.; Abbeel, P.; and Levine, S. 2018. Soft Actor-Critic: Off-Policy Maximum Entropy Deep Reinforcement Learning with a Stochastic Actor. In Dy, J.; and Krause, A., eds., *Proceedings of the 35th International Conference on Machine Learning*, volume 80 of *Proceedings of Machine Learning Research*, 1861–1870. Stockholm mässan, Stockholm Sweden: PMLR.
- Haarnoja, T.; Zhou, A.; Hartikainen, K.; Tucker, G.; Ha, S.; Tan, J.; Kumar, V.; Zhu, H.; Gupta, A.; Abbeel, P.; and Levine, S. 2019. Soft Actor-Critic Algorithms and Applications. arXiv:1812.05905.
- Hadfield-Menell, D.; Milli, S.; Abbeel, P.; Russell, S. J.; and Dragan, A. 2017. Inverse Reward Design. In Guyon, I.; Luxburg, U. V.; Bengio, S.; Wallach, H.; Fergus, R.; Vishwanathan, S.; and Garnett, R., eds., *Advances in Neural Information Processing Systems*, volume 30. Curran Associates, Inc.
- Hafner, D.; Lillicrap, T.; Ba, J.; and Norouzi, M. 2020. Dream to Control: Learning Behaviors by Latent Imagination. In *International Conference on Learning Representations*.
- Hamrick, J. B.; Bapst, V.; Sanchez-Gonzalez, A.; Pfaff, T.; Weber, T.; Buesing, L.; and Battaglia, P. W. 2020. Combining Q-Learning and Search with Amortized Value Estimates. In *8th International Conference on Learning Representations, ICLR 2020, Addis Ababa, Ethiopia, April 26-30, 2020*. OpenReview.net.

- Hamrick, J. B.; Friesen, A. L.; Behbahani, F.; Guez, A.; Viola, F.; Witherspoon, S.; Anthony, T.; Buesing, L. H.; Veličković, P.; and Weber, T. 2021. On the role of planning in model-based deep reinforcement learning. In *International Conference on Learning Representations*.
- Harris, C. R.; Millman, K. J.; van der Walt, S. J.; Gommers, R.; Virtanen, P.; Cournapeau, D.; Wieser, E.; Taylor, J.; Berg, S.; Smith, N. J.; Kern, R.; Picus, M.; Hoyer, S.; van Kerkwijk, M. H.; Brett, M.; Haldane, A.; del Río, J. F.; Wiebe, M.; Peterson, P.; Gérard-Marchant, P.; Sheppard, K.; Reddy, T.; Weckesser, W.; Abbasi, H.; Gohlke, C.; and Oliphant, T. E. 2020. Array programming with NumPy. *Nature*, 585(7825): 357–362.
- Hausman, K.; Springenberg, J. T.; Wang, Z.; Heess, N.; and Riedmiller, M. 2018. Learning an Embedding Space for Transferable Robot Skills. In *International Conference on Learning Representations*.
- Hernando, A.; Hernando, R.; Plastino, A.; and Plastino, A. R. 2013. The workings of the maximum entropy principle in collective human behaviour. *Journal of The Royal Society Interface*, 10(78): 20120758.
- Hessel, M.; Modayil, J.; van Hasselt, H.; Schaul, T.; Ostrovski, G.; Dabney, W.; Horgan, D.; Piot, B.; Azar, M. G.; and Silver, D. 2018. Rainbow: Combining Improvements in Deep Reinforcement Learning. In McIlraith, S. A.; and Weinberger, K. Q., eds., *AAAI*, 3215–3222. AAAI Press.
- Jurafsky, D.; and Martin, J. H. 2020. <https://web.stanford.edu/~jurafsky/slp3/3.pdf>. Accessed: 2021-09-09.
- Khandelwal, P.; Liebman, E.; Niekum, S.; and Stone, P. 2016. On the Analysis of Complex Backup Strategies in Monte Carlo Tree Search. In Balcan, M. F.; and Weinberger, K. Q., eds., *Proceedings of The 33rd International Conference on Machine Learning*, volume 48 of *Proceedings of Machine Learning Research*, 1319–1328. New York, New York, USA: PMLR.
- Kingma, D. P.; and Ba, J. 2015. Adam: A Method for Stochastic Optimization. In *ICLR (Poster)*.
- Kocsis, L.; and Szepesvári, C. 2006. Bandit based Monte-Carlo Planning. In *In: ECML-06. Number 4212 in LNCS*, 282–293. Springer.
- Kozakowski, P.; Januszewski, P.; Czechowski, K.; Kuciński, Ł.; and Miłoś, P. 2020. Structure and randomness in planning and reinforcement learning. In *Learning Meets Combinatorial Algorithms at NeurIPS2020*.
- Lee, C.-S.; Wang, M.-H.; Chaslot, G.; Hoock, J.-B.; Rimmel, A.; Teytaud, O.; Tsai, S.-R.; Hsu, S.-C.; and Hong, T.-P. 2009. The Computational Intelligence of MoGo Revealed in Taiwan’s Computer Go Tournaments. *Computational Intelligence and AI in Games, IEEE Transactions on*, 1: 73 – 89.
- Levine, S. 2018. Reinforcement Learning and Control as Probabilistic Inference: Tutorial and Review. arXiv:1805.00909.
- Mahlmann, T.; Togelius, J.; and Yannakakis, G. N. 2011. Towards Procedural Strategy Game Generation: Evolving Complementary Unit Types. In Di Chio, C.; Cagnoni, S.; Cotta, C.; Ebner, M.; Ekárt, A.; Esparcia-Alcázar, A. I.; Merelo, J. J.; Neri, F.; Preuss, M.; Richter, H.; Togelius, J.; and Yannakakis, G. N., eds., *Applications of Evolutionary Computation*, 93–102. Berlin, Heidelberg: Springer Berlin Heidelberg. ISBN 978-3-642-20525-5.
- Mansley, C.; Weinstein, A.; and Littman, M. L. 2011. Sample-Based Planning for Continuous Action Markov Decision Processes. In *Proceedings of the Twenty-First International Conference on International Conference on Automated Planning and Scheduling*, ICAPS’11, 335–338. AAAI Press.
- Miłoś, P.; Łukasz Kuciński; Czechowski, K.; Kozakowski, P.; and Klimek, M. 2020. Uncertainty-sensitive Learning and Planning with Ensembles. arXiv:1912.09996.
- Mnih, V.; Kavukcuoglu, K.; Silver, D.; Rusu, A. A.; Veness, J.; Bellemare, M. G.; Graves, A.; Riedmiller, M.; Fidjeland, A. K.; Ostrovski, G.; Petersen, S.; Beattie, C.; Sadik, A.; Antonoglou, I.; King, H.; Kumaran, D.; Wierstra, D.; Legg, S.; and Hassabis, D. 2015. Human-level control through deep reinforcement learning. *Nature*, 518(7540): 529–533.
- Nachum, O.; Norouzi, M.; Xu, K.; and Schuurmans, D. 2017. Bridging the Gap Between Value and Policy Based Reinforcement Learning. In Guyon, I.; Luxburg, U. V.; Bengio, S.; Wallach, H.; Fergus, R.; Vishwanathan, S.; and Garnett, R., eds., *Advances in Neural Information Processing Systems*, volume 30. Curran Associates, Inc.
- Nair, V.; and Hinton, G. E. 2010. Rectified Linear Units Improve Restricted Boltzmann Machines. In Fürnkranz, J.; and Joachims, T., eds., *ICML*, 807–814. Omnipress.
- Russell, S.; and Norvig, P. 2009. *Artificial Intelligence: A Modern Approach*. USA: Prentice Hall Press, 3rd edition. ISBN 0136042597.
- Schrittwieser, J.; Antonoglou, I.; Hubert, T.; Simonyan, K.; Sifre, L.; Schmitt, S.; Guez, A.; Lockhart, E.; Hassabis, D.; Graepel, T.; Lillicrap, T.; and Silver, D. 2020. Mastering Atari, Go, chess and shogi by planning with a learned model. *Nature*, 588: 604–609.
- Silver, D.; Hubert, T.; Schrittwieser, J.; Antonoglou, I.; Graepel, T.; Lillicrap, T.; Simonyan, K.; and Hassabis, D. 2018. A general reinforcement learning algorithm that masters chess, shogi, and Go through self-play. *Science*, 1144: 1140–1144.
- Sutton, R. 1988. Learning to Predict by the Method of Temporal Differences. *Machine Learning*, 3: 9–44.
- Sutton, R. S. 1991. Dyna, an Integrated Architecture for Learning, Planning, and Reacting. *SIGART Bull.*, 2(4): 160–163.
- Sutton, R. S.; and Barto, A. G. 2018. *Reinforcement learning: An introduction*. MIT press.
- Tanabe, Y.; Yoshizoe, K.; and Imai, H. 2009. A study on security evaluation methodology for image-based biometrics authentication systems. In *2009 IEEE 3rd International Conference on Biometrics: Theory, Applications, and Systems*, 1–6.
- Virtanen, P.; Gommers, R.; Oliphant, T. E.; Haberland, M.; Reddy, T.; Cournapeau, D.; Burovski, E.; Peterson, P.

Weckesser, W.; Bright, J.; van der Walt, S. J.; Brett, M.; Wilson, J.; Millman, K. J.; Mayorov, N.; Nelson, A. R. J.; Jones, E.; Kern, R.; Larson, E.; Carey, C. J.; Polat, İ.; Feng, Y.; Moore, E. W.; VanderPlas, J.; Laxalde, D.; Perktold, J.; Cimrman, R.; Henriksen, I.; Quintero, E. A.; Harris, C. R.; Archibald, A. M.; Ribeiro, A. H.; Pedregosa, F.; van Mulbregt, P.; and SciPy 1.0 Contributors. 2020. SciPy 1.0: Fundamental Algorithms for Scientific Computing in Python. *Nature Methods*, 17: 261–272.

Vulkan, N. 2000. An economist’s perspective on probability matching. *Journal of economic surveys*, 14(1): 101–118.

Xiao, C.; Huang, R.; Mei, J.; Schuurmans, D.; and Müller, M. 2019. Maximum Entropy Monte-Carlo Planning. In *Advances in Neural Information Processing Systems*, volume 32, 9520–9528. Curran Associates, Inc.

Ziebart, B. D. 2018. Modeling Purposeful Adaptive Behavior with the Principle of Maximum Causal Entropy.

Ziebart, B. D.; Maas, A. L.; Bagnell, J. A.; and Dey, A. K. 2008. Maximum Entropy Inverse Reinforcement Learning. In Fox, D.; and Gomes, C. P., eds., *Proceedings of the Twenty-Third AAAI Conference on Artificial Intelligence, AAAI 2008, Chicago, Illinois, USA, July 13-17, 2008*, 1433–1438. AAAI Press.

Łukasz Kaiser; Babaeizadeh, M.; Miłos, P.; Osipiński, B.; Campbell, R. H.; Czechowski, K.; Erhan, D.; Finn, C.; Kozakowski, P.; Levine, S.; Mohiuddin, A.; Sepassi, R.; Tucker, G.; and Michalewski, H. 2020. Model Based Reinforcement Learning for Atari. In *International Conference on Learning Representations*.

Appendix

Confidence intervals

We provide confidence intervals for the results using pre-trained Q-networks in Table 2.

Robustness

As an extension of our robustness experiments, we have compared the performance of the entropy and temperature parameterizations of ANTS when the hyperparameters are not tuned, but instead the score is averaged over all hyperparameter values. The results of this experiment are shown in Figure 4. The details of all robustness experiments are provided in section **Experimental details**.

Maximum entropy RL and the Legendre-Fenchel transform

In this section we introduce the Legendre-Fenchel transform, which allows to incorporate entropy types other than Shannon entropy into the maximum entropy RL framework. Maximum entropy RL using Tsallis entropy powers the ANTS-T algorithm introduced in this work, as well as the TENTS algorithm formulated by Dam et al. (2020).

Recall the maximum entropy RL objective:

$$J(\pi) = \mathbb{E}_{(s_t, a_t)} \left[\sum_{t=0}^{\infty} \gamma^t [\mathcal{R}(s_t, a_t) + \tau \mathcal{H}(\pi(\cdot|s_t))] \right] \quad (14)$$

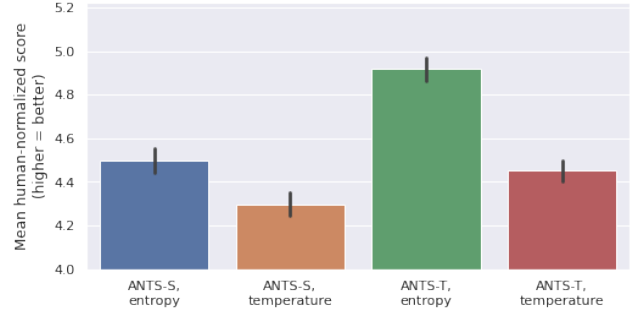


Figure 4: Mean human-normalized score averaged over hyperparameter values. We average over 24 episodes for each variant and each of the 21 games. Error bars denote 95% confidence intervals.

where \mathcal{H} is Shannon entropy and $\tau > 0$ is a temperature parameter regulating the amount of exploration. We denote the solution to the entropy-regularized RL objective as $\pi^* = \operatorname{argmax}_{\pi} J(\pi)$.

Dam et al. (2020) generalize this objective to other types of entropy and solve it using the Legendre-Fenchel transform. For a strongly convex function $\Omega : \Delta^{\mathcal{A}} \rightarrow \mathbb{R}$, where $\Delta^{\mathcal{A}} \subset \mathbb{R}^{\mathcal{A}}$ is the set of probability distributions over a finite set \mathcal{A} , the Legendre-Fenchel transform of Ω is a function $\Omega^* : \mathbb{R}^{\mathcal{A}} \rightarrow \mathbb{R}$ defined as:

$$\Omega^*(q) = \max_{\delta \in \Delta^{\mathcal{A}}} \delta \cdot q - \Omega(\delta) \quad (15)$$

where \cdot is the dot product. This maximization problem has a unique solution, which we denote as $\nabla \Omega^* : \mathbb{R}^{\mathcal{A}} \rightarrow \Delta^{\mathcal{A}}$. In the subsequent sections, we use the designation $\Omega_{\tau}(\delta) = -\tau \mathcal{H}(\delta)$ and denote its Legendre-Fenchel transform as $\Omega_{\tau}^*(q)$, and the maximizing argument (optimal policy) as $\nabla \Omega_{\tau}^*(q)$.

Dam et al. (2020) derive a backup operator, which can be used to solve entropy-regularized RL problems:

$$\begin{aligned} Q(s, a) &\leftarrow \mathcal{R}(s, a) + \gamma \mathbb{E}_{s' \sim \mathcal{P}(\cdot|s, a)} V(s') \\ V(s) &\leftarrow \Omega_{\tau}^*(Q(s, \cdot)). \end{aligned} \quad (16)$$

Fixed point iteration on this backup results in $Q = Q^*, V = V^*$, from which the optimal policy can be recovered: $\pi^*(\cdot|s) = \nabla \Omega_{\tau}^*(Q^*(s, \cdot))$. An instantiation with Shannon entropy results in *soft Q-iteration*, utilized by Haarnoja et al. (2017):

$$\begin{aligned} Q(s, a) &\leftarrow \mathcal{R}(s, a) + \gamma \mathbb{E}_{s' \sim \mathcal{P}(\cdot|s, a)} V(s') \\ V(s) &\leftarrow \tau \log \sum_{a \in \mathcal{A}} \exp \left(\frac{1}{\tau} Q(s, a) \right), \end{aligned} \quad (17)$$

with the optimal policy $\pi^*(\cdot|s) = \exp \left(\frac{1}{\tau} (Q^*(s, a) - V^*(s)) \right)$. Dam et al. (2020) utilize (16) within the MCTS framework. In the selection phase, the consecutive nodes are chosen using the E3W sampling

Table 2: Results on Atari using pretrained Q-networks with 95% confidence intervals.

	PUCT	MENTS	TENTS	ANTS-S	ANTS-T
Alien	2852.9 ± 231.95	2590.1 ± 222.34	2605.5 ± 208.74	2783.3 ± 172.0	2553.8 ± 209.9
Amidar	136.75 ± 18.25	250.6 ± 24.63	235.96 ± 19.04	147.52 ± 15.97	183.94 ± 14.51
Asterix	48505.5 ± 11038.61	8305.0 ± 1339.14	10405.5 ± 2022.98	51741.0 ± 10763.74	49758.0 ± 9791.81
Asteroids	3656.5 ± 446.97	3786.1 ± 394.0	3540.6 ± 297.11	4059.2 ± 461.43	3554.3 ± 421.79
Atlantis	278156.0 ± 3213.29	275681.0 ± 4009.21	267429.0 ± 3838.89	277870.0 ± 2554.87	280492.0 ± 2621.34
BankHeist	680.4 ± 13.63	542.5 ± 18.9	471.7 ± 19.03	706.7 ± 10.54	714.7 ± 15.32
BeamRider	21744.88 ± 1542.7	9423.6 ± 841.37	7534.24 ± 825.8	21268.46 ± 1525.12	18536.36 ± 1450.1
Breakout	388.99 ± 11.41	305.86 ± 19.37	243.22 ± 21.63	350.92 ± 15.63	377.13 ± 15.58
Centipede	18661.52 ± 3093.84	59167.26 ± 7347.34	99630.69 ± 9363.88	51387.29 ± 8853.73	133841.7 ± 9525.13
DemonAttack	55947.05 ± 2441.4	49952.2 ± 1741.16	45960.3 ± 2552.9	53998.35 ± 1813.97	53462.0 ± 1865.51
Enduro	793.99 ± 11.93	800.0 ± 0.0	800.0 ± 0.0	793.99 ± 11.93	800.0 ± 0.0
Frostbite	204.3 ± 2.76	196.5 ± 4.1	196.5 ± 4.94	179.1 ± 5.72	184.0 ± 3.66
Gopher	9605.6 ± 885.2	9330.0 ± 915.24	8150.2 ± 663.47	10770.0 ± 937.51	10766.0 ± 786.81
Hero	20714.7 ± 18.91	19939.85 ± 399.18	19845.35 ± 434.31	20617.5 ± 20.96	20443.05 ± 235.36
MsPacman	3879.7 ± 188.02	3873.4 ± 351.75	3358.4 ± 258.92	4922.7 ± 333.93	4846.1 ± 323.13
Phoenix	8875.1 ± 498.72	6788.3 ± 542.02	6857.0 ± 524.87	9187.4 ± 523.51	9557.4 ± 496.38
Qbert	15120.0 ± 31.52	13876.5 ± 481.45	13815.0 ± 493.67	15472.0 ± 93.0	15223.0 ± 108.7
Robotank	54.68 ± 3.07	26.82 ± 2.35	26.39 ± 2.23	49.22 ± 2.85	51.11 ± 2.54
Seaquest	3269.7 ± 268.31	1763.6 ± 85.33	1532.7 ± 99.31	2557.4 ± 144.53	2656.4 ± 173.15
SpaceInvaders	4629.6 ± 463.43	2042.6 ± 259.56	2023.6 ± 233.43	4713.5 ± 460.23	4453.4 ± 443.65
WizardOfWor	11834.0 ± 1357.31	7063.0 ± 994.75	8030.0 ± 1169.31	12937.0 ± 1501.01	13386.0 ± 1557.12

strategy proposed by the authors:

$$\begin{aligned} \pi_{\tau}^{\text{E3W}}(a|s) &= (1 - \lambda_s) \pi_{\tau}(a|s) + \lambda_s \frac{1}{|\mathcal{A}|}, \\ \pi_{\tau}(\cdot|s) &= \nabla \Omega_{\tau}^*(Q(s, \cdot)), \\ \lambda_s &= \frac{\epsilon |\mathcal{A}|}{\log(N(s) + 1)}, \epsilon > 0. \end{aligned} \quad (18)$$

In the simulation phase, leaves are initialized using a Q -network. In the backpropagation phase, node state values and Q -values are updated according to (16). The authors derive two new planning methods based on this procedure: TENTS, based on Tsallis entropy, and RENTS, based on relative entropy. E3W is based on the previous work of Xiao et al. (2019), which introduces E2W - a sampling strategy using the same formula, restricted to Shannon entropy, and MENTS - a planning algorithm using this strategy.

Algorithm

The pseudocode of the ANTS algorithm is shown in Algorithm 1. The function ANTS is called at every step of the episode to determine the action to take. At the beginning, the temperature $\tilde{\tau}$ is set to τ_0 . Every `adaptation_frequency` passes it is adjusted, and the Q -values in the tree are recalculated based on its new value. The temperature is transferred between episode steps. To improve efficiency, we also transfer the planning tree between steps - both for ANTS and for all baselines.

Temperature adaptation is performed by finding a root of the function defined in section **Temperature adaptation** of the main text, computed over the internal nodes, as shown in Algorithm 2. Q -values are recalculated according to (16) applied to the nodes starting from the leaves, using depth-first search.

Algorithm 1: Adaptive Entropy Tree Search.

```

function ANTS(root, model)
  for i in {1 .. n_passes} do
    (leaf, rewards) ← SELECT(root, model,  $\tilde{\tau}$ )
    leaf.children ← EXPAND(leaf, model)
     $\forall_a$  leaf.children[a].qvalue
      ← SIMULATE(leaf.state, a,  $\tilde{\tau}$ )
    BACKPROPAGATE(leaf, rewards,  $\tilde{\tau}$ )
    if i mod adaptation_frequency = 0 then
       $\tau$  ← ADAPT_TEMPERATURE(root)
       $\tilde{\tau}$  ← exp( $\alpha \log \tilde{\tau} + (1 - \alpha) \log \tau$ )
      RECALCULATE_QVALUES(root,  $\tilde{\tau}$ )
    end if
  end for
  return FINAL_ACTION(root,  $\tilde{\tau}$ )
end function

```

The selection phase is shown in Algorithm 3. It selects actions inside the tree by sampling from the E3W policy (5). We also limit the length of the path using a hyperparameter `depth_limit`. This is omitted from the pseudocode for clarity.

We omit the expansion phase for brevity. In the simulation phase, we just run the Q -network. In the backpropagation phase, we traverse the selected path bottom-up and update the Q -values, as shown in Algorithm 4.

We sample the final action from the E3W policy, rescaled by the action selection temperature τ_{sel} , as shown in Algorithm 5. In the pretrained Q -network experiments, we set τ_{sel} to a very low value, so this is equivalent to `argmax` with random tie breaking.

Algorithm 2: Temperature adaptation.

```

function ADAPT_TEMPERATURE(root)
  function EXCESS_ENTROPY( $\tau$ )
    nodes  $\leftarrow$  INTERNAL_NODES(root)
     $\forall n \in \text{nodes} \forall a \in \mathcal{A} \ q[n, a] \leftarrow n.\text{children}[a].\text{qvalue}$ 
     $\forall n \in \text{nodes} \ h[n] \leftarrow \mathcal{H}(\nabla \Omega_{\tau}^*(q[n, \cdot]))$ 
    return  $\left( \frac{1}{|\text{nodes}|} \sum_{n \in \text{nodes}} h[n] \right) - \mathcal{H}_{\text{avg}}$ 
  end function
  return  $\text{max}(\tau_{\text{min}}, \text{FIND\_ROOT}(\text{EXCESS\_ENTROPY}))$ 
end function

function RECALCULATE_QVALUES(node,  $\tau$ )
  for child in node.children do
    RECALCULATE_QVALUES(child,  $\tau$ )
  end for
  node.qvalue  $\leftarrow$  QVALUE(node,  $\tau$ )
end function

```

Complexity analysis

We first consider a variant of the algorithm without transferring the tree between steps. We denote $n = \text{n_passes}$, $m = \text{n_passes/adaptation_frequency}$, $d = \text{depth_limit}$ and $A = |\mathcal{A}|$. In each call of ANTS we perform n planning passes. In each pass, we traverse a path of length $O(d)$, choosing an action out of A in each node. This gives us a time complexity of $O(ndA)$ for running the MCTS phases. Additionally, in m of the passes we perform temperature adaptation. We assume that the optimization only requires a constant number of steps. In each step, we compute the entropies of all internal nodes in the tree. There is n of them - each has been expanded in some previous planning pass. Computing the entropy takes $O(A)$ time. Hence, the time complexity of temperature adaptation is $O(mnA)$, and the time complexity of the whole algorithm is $O(nA(d + m))$. We only need to store the tree in memory. Each node stores links to its A children, and we have n internal nodes, so the space complexity is $O(nA)$.

In the case of keeping the tree between episode steps, the tree can grow up to $O(nd)$ nodes - in each pass we expand n nodes, and we can only "see" nodes expanded in the last d steps. All other considerations stay the same as in the previous variant, which yields a time complexity of $O(ndA)$ for the MCTS phases and $O(nmdA)$ for temperature adaptation, so $O(nmdA)$ in total, and a space complexity of $O(ndA)$. However, note that keeping the tree is an optimization, achieved by reusing the computation performed in the previous episode steps. As such, when keeping the tree, the number of passes can be reduced to match the performance of the variant without keeping the tree, and then the final runtime should be lower.

Experimental details

We perform our experiments on 21 Atari games from the Arcade Learning Environment. We apply the following preprocessing to those environments:

Algorithm 3: Selection phase.

```

function SELECT(root, model,  $\tau$ )
  node  $\leftarrow$  root
  state  $\leftarrow$  root.state
  rewards  $\leftarrow$  ()
  while not IS_LEAF(node) do
    action  $\leftarrow$  TREE_ACTION(node,  $\tau$ )
    (state, reward)  $\leftarrow$  model(state, action)
    rewards  $\leftarrow$  rewards  $\oplus$  (reward)
    node  $\leftarrow$  node.children[action]
  end while
  return (node, rewards)
end function

function TREE_ACTION(node,  $\tau$ )
  sample  $a \sim$  E3W_POLICY(node,  $\tau$ )
  return a
end function

function E3W_POLICY(node,  $\tau$ )
   $\lambda \leftarrow \epsilon |\mathcal{A}| / \log(\text{node.count} + 1)$ 
   $\forall a \in \mathcal{A} \ q[a] \leftarrow \text{node.children}[a].\text{qvalue}$ 
   $\pi_{\text{if}}[\cdot] \leftarrow \nabla \Omega_{\tau}^*(q[\cdot])$ 
  return  $(1 - \lambda)\pi_{\text{if}}[\cdot] + \lambda \frac{1}{|\mathcal{A}|}$ 
end function

```

Algorithm 4: Simulation and backpropagation phases.

```

function SIMULATE(state, action,  $\tau$ )
  return  $\hat{Q}(\text{state}, \text{action}, \tau)$ 
end function

function BACKPROPAGATE(node, rewards,  $\tau$ )
  for reward in REVERSED(rewards) do
    node.reward  $\leftarrow$  reward
    node.count  $\leftarrow$  node.count + 1
    node.qvalue  $\leftarrow$  QVALUE(node,  $\tau$ )
    node  $\leftarrow$  node.parent
  end for
end function

```

- Repeating each action for 4 consecutive steps, taking a pixelwise maximum of 2 last frames as the observation.
- Stacking 4 last frames obtained from the previous step in one observation.
- Gray-scale observations, cropped and rescaled to size 84×84 .
- A random number of no-op actions from range $[0..30]$ at the beginning of each episode.
- Time limit of 10K interactions with the environment for the pretrained Q-network experiments, 1K for the closed-loop experiments.

We do not use reward clipping in any of the experiments.

To be able to make the best use of computation time, we retain the planning tree between interactions with the environment. In MENTS and TENTS, we initialize the leaves as:

Algorithm 5: Choosing the final action.

```
function FINAL_ACTION(node,  $\tau$ )
  sample  $a \sim \text{E3W\_POLICY}(node, \tau \cdot \tau_{\text{sel}})$ 
  return  $a$ 
end function
```

$$Q(s, a) \leftarrow \left(\hat{Q}(s, a) - \Omega_{\tau_{\text{init}}}^*(\hat{Q}(s, \cdot)) \right) / \tau_{\text{init}}, \quad (19)$$

In PUCT, we initialize the Q-values as $Q(s, a) = \hat{Q}(s, a)$ and the prior policy as $\pi_{\text{prior}}(a|s) \propto \exp(\hat{Q}(s, a) / \tau_{\text{init}})$.

Hyperparameters

In order to provide a fair comparison between algorithms, we have used exactly the same amount of computation for tuning all algorithms evaluated in this work. Tuning was performed in the pretrained Q-network setup, and the chosen hyperparameters were used as a base for all other experiments.

Pretrained Q-networks We have considered the following sets of hyperparameter values for individual algorithms:

PUCT:

- c - exploration parameter: $\{0.003, 0.01, 0.03, 0.1, 0.3, 1.0, 3.0, 10.0\}$

- τ_{init} - prior policy temperature: $\{0.001, 0.01, 0.1, 1.0\}$

MENTS and TENTS:

- τ - planning temperature: $\{0.001, 0.003, 0.01, 0.03, 0.1, 0.3, 1.0, 3.0, 10.0, 30.0, 100.0, 300.0, 1000.0\}$
- ϵ - exploration parameter in (5): $\{0.001, 0.01, 0.1\}$
- τ_{init} - leaf initialization temperature in (10): $\{0.001, 0.01, 0.1, 1.0\}$

ANTS-S and ANTS-T:

- \mathcal{H}_{avg} - target average entropy:
 - ANTS-S: $\{0.2, 0.5, 1.0, 1.5\}$
 - ANTS-T: $\{0.02, 0.05, 0.1, 0.2\}$
- τ_{min} - minimum temperature in Algorithm 2: $\{0.01, 0.001, 0.0001\}$
- τ_0 - starting temperature: $\{1.0, 10.0, 100.0\}$
- ϵ - exploration parameter in (5): $\{0.001, 0.01, 0.1, 1.0\}$
- α - temperature smoothing factor: $\{0.5, 0.8, 0.9\}$
- `adaptation_frequency` - number of MCTS passes between temperature adaptations: $\{10, 20, 50, 100\}$

The ranges of \mathcal{H}_{avg} are different for ANTS-S and ANTS-T, because the values of maximum possible entropy differ for Shannon and Tsallis entropy.

To make α and `adaptation_frequency` independent, we have adjusted the smoothing parameter α so that it corresponds to the total decay applied in a single call of Algorithm 1, regardless of the value of `adaptation_frequency`: $\alpha' = \alpha^{m/n}$, where $n = \text{n_passes}$ and $m = \text{adaptation_frequency}$.

We were able to tune PUCT exhaustively using grid search, because it only has 2 hyperparameters. For the rest of the algorithms we have used random search. In all cases, the computational budget was 32 experiments per game, per algorithm. For each algorithm, we have chosen the hyperparameter set maximizing the average human-normalized score across the 21 games:

$$S_{\text{hnorm}} = \frac{S_{\text{raw}} - S_{\text{random}}}{S_{\text{human}} - S_{\text{random}}}, \quad (20)$$

where S_{raw} is the raw, unnormalized score, S_{human} is the average human score and S_{random} is the average score of a uniform policy. We have used the same human and random scores as Badia et al. (2020).

The chosen hyperparameter sets are:

- PUCT: $c = 1.0, \tau_{\text{init}} = 1.0$
- MENTS: $\tau = 1.0, \epsilon = 0.001, \tau_{\text{init}} = 0.01$
- TENTS: $\tau = 3.0, \epsilon = 0.001, \tau_{\text{init}} = 0.1$
- ANTS-S: $\mathcal{H}_{\text{avg}} = 0.2, \tau_{\text{min}} = 0.01, \tau_0 = 10.0, \epsilon = 0.01, \alpha = 0.9, \text{adaptation_frequency} = 50$
- ANTS-T: $\mathcal{H}_{\text{avg}} = 0.2, \tau_{\text{min}} = 0.001, \tau_0 = 100.0, \epsilon = 0.01, \alpha = 0.5, \text{adaptation_frequency} = 20$

We have set the number of MCTS passes to 100 and a depth limit of 50 for all algorithms.

Planning and learning For the planning and learning experiments we have set the number of MCTS passes to 30 and the depth limit to 20. The rest of the hyperparameters were set to the same values as described in the previous section. We have additionally tuned the selection temperature τ_{sel} using exhaustive search on the set $\{0.1, 0.2, 0.5, 1.0\}$, separately for PUCT, MENTS, TENTS, ANTS-S and ANTS-T. In each case, we have chosen the value maximizing the median out of three seeds of the average human-normalized score computed over five randomly-selected games: Enduro, Atlantis, MsPacman, Asteroids and Robotank.

The selected values are:

- PUCT: $\tau_{\text{sel}} = 0.2$
- MENTS: $\tau_{\text{sel}} = 0.5$
- TENTS: $\tau_{\text{sel}} = 0.5$
- ANTS-S: $\tau_{\text{sel}} = 0.5$
- ANTS-T: $\tau_{\text{sel}} = 0.5$

In the closed-loop training experiments, we use a down-scaled version of the architecture from (Mnih et al. 2015), with temperature injection after the last hidden layer:

1. Convolution of depth 16, kernel size 8, stride 4.
2. Convolution of depth 16, kernel size 4, stride 2.
3. Convolution of depth 16, kernel size 3, stride 1.
4. Flattening to a vector.
5. Dense layer of depth 64.
6. Temperature injection (see below).
7. Dense layer predicting the action Q-values.

For the temperature injection, we take a logarithm of the temperature, apply a linear layer of depth 64 and merge the two inputs using layer normalization (Ba, Kiros, and Hinton 2016) followed with an element-wise sum.

All activations are rectified linear units (Nair and Hinton 2010). We train the networks using the Adam optimization algorithm (Kingma and Ba 2015) with learning rate 0.001. The networks are trained using L2 loss with the Q-values calculated by the planner for the root nodes. For PUCT, we learn both the Q-value predictor and the prior policy as separate heads. The policy head is trained using cross-entropy loss with the child visitation distribution.

In each training epoch we collect 24 episodes and add them into the replay buffer, and then apply 1000 network updates on random minibatches sampled from the replay buffer. We use batch size 64. The buffer holds 30000 interactions with the environment. At the beginning of the experiment, we fill the replay buffer with episodes collected using untrained networks.

Robustness For the temperature parameterization, the set of τ values is $\{0.001, 0.003, 0.01, 0.03, 0.1, 0.3, 1.0, 3.0, 10.0\}$ - approximately equidistant in log-space, with endpoints chosen as the minimum and maximum temperature value that worked best on some game when tuning the MENTS algorithm.

The set of \mathcal{H}_{avg} values for the entropy parameterization was chosen to be of the same size, to ensure a fair comparison. It spans the $(0, \mathcal{H}_{\text{max}})$ interval. The maximum possible entropy \mathcal{H}_{max} for ANTS-S is around 3, and for ANTS-T is around 0.5, which results in the set $\{0.3, 0.6, 0.9, 1.2, 1.5, 1.8, 2.1, 2.4, 2.7\}$ for ANTS-S and $\{0.05, 0.1, 0.15, 0.2, 0.25, 0.3, 0.35, 0.4, 0.45\}$ for ANTS-T.

Ablations In the MENTS-EVAL ablation, we tune τ_{init} from the set $\{0.001, 0.01, 0.1, 1.0\}$. The chosen value is 0.01.

Temperature visualization

To provide insight into how the mechanism of temperature adaptation in ANTS-S and ANTS-T behaves in practice, we have plotted the temperature changes throughout an episode for each of the 21 games. Those plots are shown in Figure 6. For both variants of ANTS we have set the minimum temperature $\tau_{\text{min}} = 0.001$ to ensure that the plots are comparable. We have observed that the patterns of temperature changes vary significantly between games. For instance, the temperature in Enduro cyclically switches between low and high values. In BreamRider we can see cyclical spikes. In Breakout we can see a spike near the beginning of the episode, after which the temperature drops and remains approximately constant for the rest of the episode.

We have further investigated the cause of the spike in Breakout, and determined that it is due to the changing scale of the returns, which provides evidence that ANTS is able to successfully adapt to such changes. Breakout is a classical Atari game, in which the player controls a paddle at the bottom of the screen, which bounces off a ball. The ball hits and destroys bricks at the top of the screen. A reward

is given for each brick, and the game is finished when all bricks are gone. As we can see in Figure 5, in the period before the spike, the ball bounces between the paddle and the bricks at the bottom, which gives rewards at a low frequency. At the spike, a passage is opened to the empty space at the top of the screen and the ball goes there. There, the ball rapidly bounces between the top of the screen and the top bricks, which gives rewards at a high frequency. The end of the spike corresponds to the final stage of the episode, when most of the bricks are gone and the ball bounces freely over the screen. At that stage, the speed of the game is increased, so the reward frequency is higher than at the beginning, which is reflected in the higher temperature.

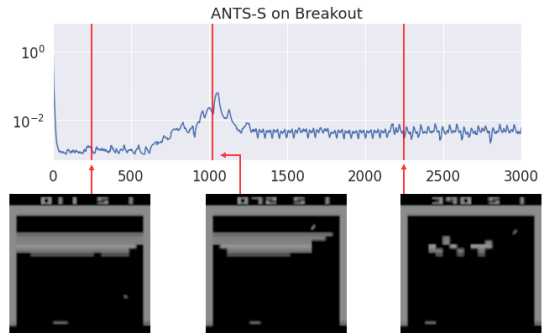


Figure 5: Temperature changes in a random episode of Breakout played by ANTS-S. Episode steps are shown at the X axis, and the temperature is shown at the Y axis. The spike appears when the ball enters the empty corridor at the top of the screen.

Infrastructure and runtime

For our experiments we have used machines with two Intel Xeon E5-2697 v3 2.6 GHz CPU processors and 128 GB memory. We have run two parallel experiments on a single machine, so one experiment has used one processor on average. We have not used any GPUs - with our relatively small neural networks we have found the performance gain to be minor.

A single experiment with pretrained Q-networks takes around 8 hours on average (100 episodes). A single experiment for hyperparameter tuning or for the ablations takes around 2 hours (24 episodes). A single closed-loop training experiment takes around 144 hours.

In total, we have used approximately:

- 6700 CPU-hours for hyperparameter tuning with pretrained Q-networks
- 14000 CPU-hours for tuning τ_{sel} for the planning-learning experiments
- 76000 CPU-hours for the planning-learning experiments
- 840 CPU-hours for generating Table 2
- 1500 CPU-hours for the robustness experiments
- 250 CPU-hours for the ablations

Which results in around 99000 CPU-hours for all experiments.

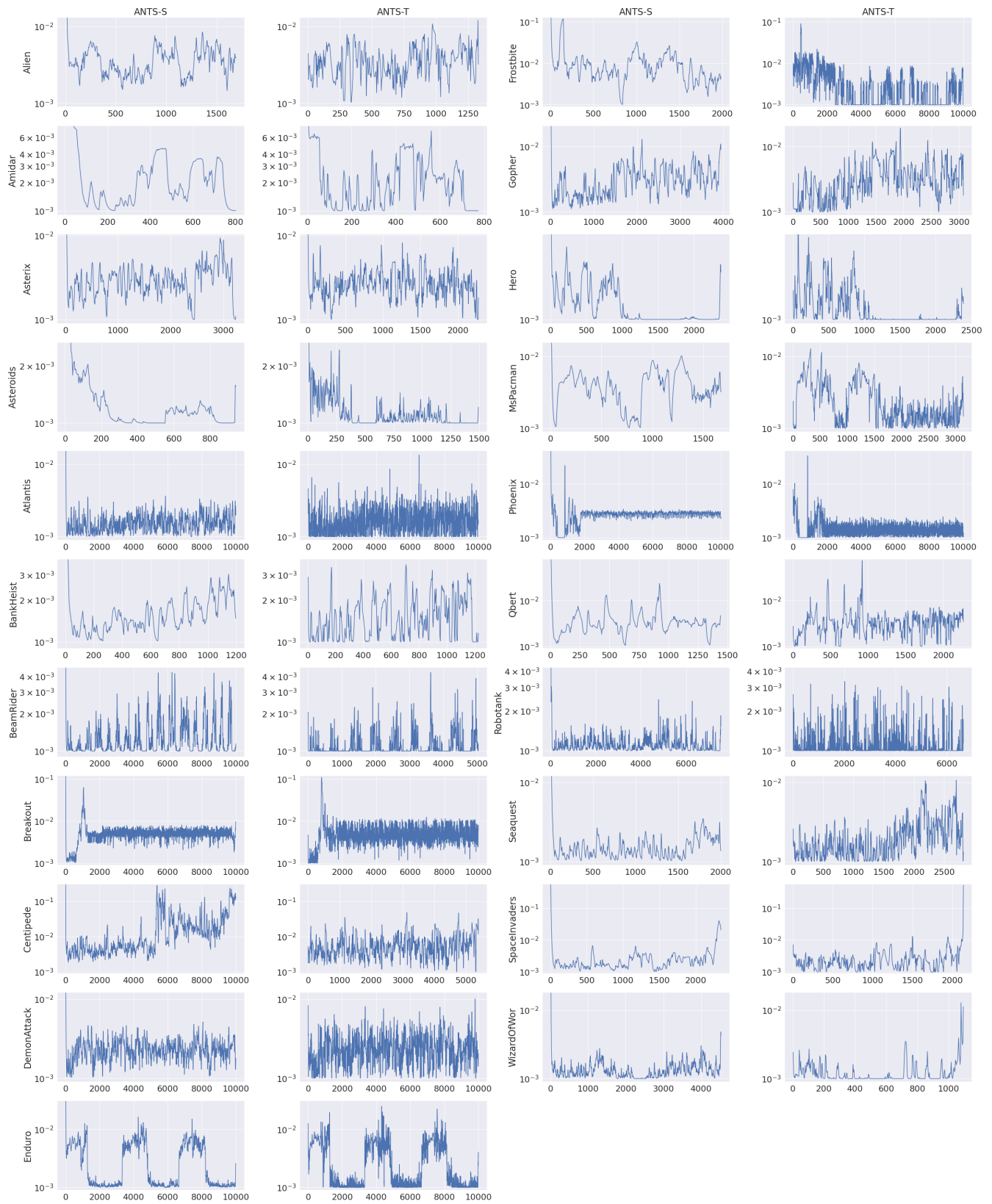


Figure 6: Temperature changes during random episodes of the 21 Atari games played by ANTS-S and ANTS-T. Episode steps are shown at the X axes, and the temperature is shown at the Y axes.

Code

The code and hyperparameter settings used to run all experiments in this work are in a code repository in supplementary material. We use pretrained Q-networks from the Dopamine library (Castro et al. 2018), released under Apache-2.0 license.

Software dependencies:

- cloudpickle (<https://github.com/cloudpipe/cloudpickle>): BSD 3-Clause license
- Gin Config (<https://github.com/google/gin-config>): Apache-2.0 license
- joblib (<https://github.com/joblib/joblib>): BSD 3-Clause license
- Numpy (Harris et al. 2020): BSD 3-Clause license
- OpenAI Gym (Brockman et al. 2016): MIT license
- SciPy (Virtanen et al. 2020): BSD 3-Clause license
- tblib (<https://github.com/ionelmc/python-tblib>): BSD 2-Clause license
- TensorFlow (Abadi et al. 2016): Apache-2.0 license

Theoretical analysis

In this section, we present theoretical analysis of our approach. We assume a model in which temperature τ_t is controlled extrinsically and obeys

$$|\tau_t - \tau| \leq C \cdot 1/\log t, \quad (21)$$

for $C > 0$. This is a simplifying assumption. We note, however, that we require a slow convergence at rate $O(1/\log t)$. Our main results, Theorem 2, states that the E2W sampling strategy introduced below ensures fast convergence of value estimates, so that with exponentially decreasing probability the greedy policy chooses the optimal action. The analysis is based on (Xiao et al. 2019).

Definitions The basic setup is that of bandit theory. Assume $K \in \mathbb{N}$ to be the number of arms (actions). Each arm a has associated a random (reward) distribution ν_a and $\mathbf{r} \in \mathbb{R}^K$ is the corresponding mean reward vector. The distributions ν_a are assumed to be sub-gaussian with the variance smaller than some σ^2 .

Importantly, we assume that max-entropy target, namely

$$\max_{\pi} \{\pi \cdot \mathbf{r} + \tau \mathcal{H}(\pi)\}, \quad \tau > 0,$$

where \cdot denotes the scalar product and $\mathcal{H}(\pi) := -\sum_{i=1}^K \pi(i) \log \pi(i)$ is the entropy of the distribution π . Note that, when the temperature τ is set to 0 we recover the standard RL objective. Here, we always assume $\tau > 0$ adhering to the max-entropy principle. Moreover, as proved in (Xiao et al. 2019), the entropy regularization yields an exponential convergence. This property is also enjoyed by our model, see Theorem 2. Define the soft indmax and softmax functions:

$$\begin{aligned} \mathbf{f}_{\tau}(\mathbf{r}) &= \exp\{(\mathbf{r} - \mathcal{F}_{\tau}(\mathbf{r}))/\tau\}, \\ \mathcal{F}_{\tau}(\mathbf{r}) &= \tau \log \sum_{i=1}^K \exp(r(i)/\tau). \end{aligned} \quad (22)$$

The following Lipschitz properties holds

Lemma 1. For any $\mathbf{r}_1, \mathbf{r}_2 \in \mathbb{R}^K$ and $\tau > 0$ we have

$$\|\mathbf{f}_{\tau}(\mathbf{r}_1) - \mathbf{f}_{\tau}(\mathbf{r}_2)\|_{\infty} \leq \frac{2}{\tau} \|\mathbf{r}_1 - \mathbf{r}_2\|_{\infty}.$$

Moreover, for any $\tau > 0$ there exists C_{τ} such that for any $\tau_1, \tau_2 \geq \tau$ and $\mathbf{r} \in \mathbb{R}^K$ we have

$$\|\mathbf{f}_{\tau_1}(\mathbf{r}) - \mathbf{f}_{\tau_2}(\mathbf{r})\|_{\infty} \leq C_{\tau} |\tau_1 - \tau_2|. \quad (23)$$

Proof. Using (22) we write

$$\begin{aligned} \|\mathbf{f}_{\tau}(\mathbf{r}_1) - \mathbf{f}_{\tau}(\mathbf{r}_2)\|_{\infty} &\leq \|\log \mathbf{f}_{\tau}(\mathbf{r}_1) - \log \mathbf{f}_{\tau}(\mathbf{r}_2)\|_{\infty} \\ &= \frac{1}{\tau} \|\mathbf{r}_1 - \mathbf{r}_2\|_{\infty} \\ &\quad + \left| \log \sum_{i=1}^K \exp(r_1(i)/\tau) - \log \sum_{i=1}^K \exp(r_2(i)/\tau) \right|. \end{aligned}$$

It is straightforward to check that $\nabla_{\mathbf{r}} \mathcal{F}_{\tau}(\mathbf{r}) = [\exp(r(1)/\tau)/Z, \dots, \exp(r(K)/\tau)/Z]$, where $Z = \sum_{i=1}^K \exp(r(i)/\tau)$. Therefore, $\|\nabla_{\mathbf{r}} \mathcal{F}_{\tau}(\mathbf{r})\|_{\infty} \leq 1$ and consequently $|\mathcal{F}_{\tau}(\mathbf{r}_1) - \mathcal{F}_{\tau}(\mathbf{r}_2)| \leq \|\mathbf{r}_1 - \mathbf{r}_2\|$.

We switch to the proof of (23). Using (22) we get

$$\begin{aligned} \|\mathbf{f}_{\tau_1}(\mathbf{r}) - \mathbf{f}_{\tau_2}(\mathbf{r})\|_{\infty} &\leq \|\log \mathbf{f}_{\tau_1}(\mathbf{r}) - \log \mathbf{f}_{\tau_2}(\mathbf{r})\|_{\infty} \\ &= \left| \frac{1}{\tau_1} - \frac{1}{\tau_2} \right| \|\mathbf{r}\|_{\infty} \\ &\quad + \left| \log \sum_{i=1}^K \exp(r(i)/\tau_1) - \log \sum_{i=1}^K \exp(r(i)/\tau_2) \right|. \end{aligned}$$

The rest of the proof follows by the fact that the derivative of $\sigma \mapsto \log \sum_i \exp(r(i)/\sigma)$ is bounded, when $\sigma \geq \tau$. \square

Estimators and E2W sampling Let $\{A_t\}$ be a random sequence of arm choices. We denote the empirical frequency and reward estimator

$$\begin{aligned} N_t(a) &= \sum_{i=1}^t \mathbb{I}\{A_i = a\}, \\ \hat{\mathbf{r}}_t(a) &= \sum_{i=1}^t \mathbb{I}\{A_i = a\} R_i / N_t(a), \end{aligned} \quad (24)$$

where R_i are sampled independently from distribution ν_{A_i} .

Xiao et al. (2019) introduced the empirical exponential weight (E2W) sampling strategy:

$$\pi_t^{\tau}(a) = (1 - \lambda_t) \mathbf{f}_{\tau}(\hat{\mathbf{r}}_t)(a) + \frac{\lambda_t}{K}, \quad (25)$$

where $\lambda_t = K/\log(t+1)$.

Concentration results Assume that we use the above sampling strategy with variable τ_t . Further, for $\epsilon > 0$ we define

$$\begin{aligned} E_{\epsilon} &= \left\{ \left| \tilde{N}_t(a) - N_t(a) \right| < \epsilon, \forall a \in \{1, \dots, K\} \right\}, \\ \tilde{N}_t(a) &= \mathbb{E} N_t(a) = \sum_{s=1}^t \pi_s^{\tau_s}. \end{aligned} \quad (26)$$

We observe that $N_t(a)$ are well-concentrated, namely

$$\mathbb{P}(E_\epsilon^c) \leq 2K \exp\left(-\frac{2\epsilon^2}{t}\right). \quad (27)$$

The proof is a straightforward application of the union bound and application of Hoeffding's inequality. The particular choice of λ_t in (25) ensures enough exploration to obtain sharp estimates of rewards. This is summarized by the following key lemma.

Lemma 2. *Assume the stochastic softmax bandit problem (recall that we assume sub-gaussian reward distributions). Then E2W can guarantee that for some $C > 0$ and $t \geq 4$ we have*

$$\begin{aligned} & \mathbb{P}\left(\|\mathbf{r} - \hat{\mathbf{r}}_t\|_\infty \geq \frac{2\sigma}{\log(2+t)}\right) \\ & \leq C \exp\left(-\frac{t}{(\log(2+t))^3}\right). \end{aligned}$$

Proof. By the choice of λ_t in (25), it follows that for all a and $t \geq 4$

$$\begin{aligned} \tilde{N}_t(a) &= \sum_{s=1}^t \pi_s(a) \geq \sum_{s=1}^t \frac{1}{\log(1+s)} \\ &\geq \sum_{s=1}^t \frac{1}{\log(1+s)} - \frac{s/(s+1)}{(\log(1+s))^2} \\ &\geq \int_1^{1+t} \frac{1}{\log(1+s)} - \frac{s/(s+1)}{(\log(1+s))^2} ds \\ &= \frac{1+t}{\log(2+t)} - \frac{1}{\log 2} \geq \frac{t}{2\log(2+t)}. \end{aligned}$$

Recall (27) and set $\epsilon = \frac{t}{4\log(2+t)}$. On E_ϵ it follows that $N_t(a) \geq \frac{t}{4\log(2+t)}$. Then by sub-gaussianness for any $\delta > 0$ we get

$$\begin{aligned} & \mathbb{P}\left(|\mathbf{r}(a) - \hat{\mathbf{r}}_t(a)| > \sqrt{\frac{8\sigma^2 \log\left(\frac{2}{\delta}\right) \log(2+t)}{t}} \middle| E_\epsilon\right) \\ & \leq \mathbb{P}\left(|\mathbf{r}(a) - \hat{\mathbf{r}}_t(a)| > \sqrt{\frac{2\sigma^2 \log\left(\frac{2}{\delta}\right)}{N_t(a)}} \middle| E_\epsilon\right) \leq \delta. \end{aligned} \quad (28)$$

Let δ satisfy that $\log(2/\delta) = \frac{t}{(\log(2+t))^3}$, then

$$\begin{aligned} & \mathbb{P}\left(|\mathbf{r}(a) - \hat{\mathbf{r}}_t(a)| > \frac{2\sigma}{\log(2+t)}\right) \\ & \leq 2 \exp\left(-\frac{t}{(\log(2+t))^3}\right) \end{aligned}$$

Therefore, by (27) and (28) we get

$$\begin{aligned} & \mathbb{P}\left(\|\mathbf{r}_t - \hat{\mathbf{r}}_t\|_\infty \geq \frac{2\sigma}{\log(2+t)}\right) \\ & \leq \mathbb{P}\left(\|\mathbf{r}_t - \hat{\mathbf{r}}_t\|_\infty \geq \frac{2\sigma}{\log(2+t)} \mid E_\epsilon\right) + \mathbb{P}(E_\epsilon^c) \\ & \leq \sum_{a=1}^K \mathbb{P}\left(|\mathbf{r}(a) - \hat{\mathbf{r}}_t(a)| > \frac{2\sigma}{\log(2+t)} \mid E_\epsilon\right) + \mathbb{P}(E_\epsilon^c) \\ & \leq 2K \exp\left(-\frac{t}{(\log(2+t))^3}\right) \\ & \quad + 2K \exp\left(-\frac{t}{2(\log(2+t))^2}\right) \\ & \leq 4K \exp\left(-\frac{t}{(\log(2+t))^3}\right). \end{aligned}$$

□

Convergence in the bandit problem We consider the softmax bandit problem and assume that the temperature varies according to (21). More precisely, we use the E2W scheme $\pi_t^{\tau_t}$. Recall that by (22) the optimal softmax policy is $\mathbf{f}_\tau(\mathbf{r})$. The following analogue of (Xiao et al. 2019, Theorem 3) holds.

Theorem 1. *Consider E2W applied to the stochastic softmax bandit problem. Let $N_t^* := \mathbf{f}_\tau(\mathbf{r}) \cdot t$. Then there exist some constants $C_1, C_2 > 0$ such that*

$$\begin{aligned} & \mathbb{P}(\mathcal{O}_t) \leq C_2 t \exp\left\{-\frac{t}{(\log t)^3}\right\}, \\ & \mathcal{O}_t := \left\{|N_t(a) - N_t^*(a)| > \frac{C_1 t}{\log t}, \forall a \in \{1, \dots, K\}\right\}. \end{aligned} \quad (29)$$

Proof. Fix a and recall (26). We define auxiliary $\bar{N}_t^* = \sum_{s=1}^t \mathbf{f}_{\tau_s}(\mathbf{r})$. By the triangle inequality we have

$$|\tilde{N}_t(a) - N_t^*(a)| \leq |\tilde{N}_t(a) - \bar{N}_t^*(a)| + |\bar{N}_t^*(a) - N_t^*(a)|. \quad (30)$$

The second term can be easily handled by Lemma 1

$$\begin{aligned} |\bar{N}_t^*(a) - N_t^*(a)| &\leq \sum_{s=1}^t \|\mathbf{f}_{\tau_s}(\mathbf{r}) - \mathbf{f}_\tau(\mathbf{r})\| \\ &\leq C_1 \sum_{s=1}^t |\tau_s - \tau| \\ &\leq C_2 \sum_{s=1}^t \frac{1}{\log(s+1)} \\ &\leq C_3 \frac{t}{\log(t+1)}, \end{aligned} \quad (31)$$

for some constants $C_1, C_2, C_3 > 0$. To deal with $|\tilde{N}_t(a) - \bar{N}_t^*(a)|$ we denote the following event

$$\mathcal{G}_t = \left\{\|\mathbf{r} - \hat{\mathbf{r}}_t\|_\infty < \frac{2\sigma}{\log(2+t)}\right\}, \quad (32)$$

(recall that $\hat{\mathbf{r}}_t$ is given by (24) and σ is the upperbound of the variances of the reward distributions).

We bound $|\tilde{N}_t(a) - \bar{N}_t^*(a)|$, on the event $\bigcap_{s=1}^t \mathcal{G}_t$ and for $t \geq 4$:

$$\begin{aligned} |\tilde{N}_t(a) - \bar{N}_t^*(a)| &= \sum_{s=1}^t |\pi_s^{\tau_s}(a) - \mathbf{f}_{\tau_s}(\mathbf{r})(a)| \\ &\leq \sum_{s=1}^t |\mathbf{f}_{\tau_s}(\hat{\mathbf{r}}_s)(a) - \mathbf{f}_{\tau_s}(\mathbf{r})(a)| + \sum_{s=1}^t \lambda_s \\ &\leq \frac{2}{\min_s \tau_s} \sum_{s=1}^t \|\hat{\mathbf{r}}_s - \mathbf{r}\|_\infty + \sum_{s=1}^t \lambda_s \\ &\leq \frac{2}{\min_s \tau_s} \sum_{s=1}^t \frac{2\sigma}{\log(2+s)} + \sum_{s=1}^t \lambda_s, \end{aligned}$$

where in the second inequality we used Lemma 1. Recalling definition of λ_s in (25) we easily get $|\tilde{N}_t(a) - \bar{N}_t^*(a)| \mathbf{1}_{\bigcap_{s=1}^t \mathcal{G}_t} \leq C_4 t / \log t$ for some $C_4 > 0$. Employing the union bound and Lemma 2 we get

$$\begin{aligned} &\mathbb{P}\left(|\tilde{N}_t(a) - \bar{N}_t^*(a)| > \frac{C_4 t}{\log t}\right) \\ &\leq \sum_{s=1}^t \mathbb{P}(\mathcal{G}_s^c) = \sum_{s=1}^t C_5 \exp\left\{-\frac{t}{(\log(s+2))^3}\right\} \\ &\leq C_6 t \exp\left(-\frac{t}{(\log(2+t))^3}\right), \end{aligned}$$

for some $C_5, C_6 > 0$. Recalling (30) and (31) we get that for some $C_7 > 0$ we have

$$\begin{aligned} &\mathbb{P}\left(|\tilde{N}_t(a) - N_t^*(a)| > \frac{C_7 t}{\log t}\right) \\ &\leq C_6 t \exp\left\{-\frac{t}{(\log(2+t))^3}\right\}. \end{aligned}$$

Now the result of the theorem follows applying (27) and standard utilization of the union bound. \square

Let now consider the optimal action $a^* = \operatorname{argmax}_a \mathbf{r}(a)$. Importantly, the E2W exploration ensures fast (exponential) convergence of the value estimates, so that the greedy policy chooses a^* with high probability.

Theorem 2. *Consider greedy policy*

$$a_t^* := \operatorname{argmax}_a \mathbf{f}_\tau(\hat{\mathbf{r}}_t)(a).$$

Then, there exists $C_1, C_2 > 0$ such that

$$\mathbb{P}(a_t^* \neq a^*) \leq C_1 \exp\left(-C_2 \frac{t}{(\log(t+2))^3}\right).$$

Proof. The proof is rather easy consequence of the already proven facts. Indeed, let $\Delta > 0$ be the difference of the highest reward (i.e. $\max_a \mathbf{r}(a) = \mathbf{r}(a^*)$). We may assume that \mathcal{O}_t in (29) holds. This implies, by Lemma 2 that the errors of empirical estimates $\|\hat{\mathbf{r}}_t - \mathbf{r}\|_\infty < \Delta$, for t large enough. \square